Nano Energy 96 (2022) 107065

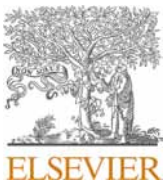

Contents lists available at ScienceDirect

Nano Energy

journal homepage: www.elsevier.com/locate/nanoen

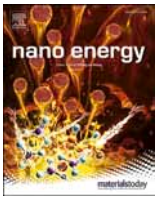

Useful spontaneous hygroelectricity from ambient air by ionic wood

Yang Li, Jiedong Cui, Haoyu Shen, Chaocheng Liu, Peilin Wu, Zhiyun Qian, Yulong Duan, Detao Liu *

School of Light Industry and Engineering, South China University of Technology, Wushan Rd., 381#, Tianhe District, Guangzhou, Guangdong 510640, China

ARTICLE INFO

Keywords:
Ionic wood
Hygroelectricity
Ambient air
Stability
Sustainability

ABSTRACT

Spontaneous electricity generator using moisture in ambient air has been developed rapidly in recent years for its great potential in self-sustained systems. However, due to the lack of efficient and continuous ion transport, the power-generation ability and stability from existing materials are unsatisfactory (ultra-low current, intermittent voltage and strong dependence on moisture) for practical applications. Here we report a generator made of ionic wood processed from natural wood using a simple and effective strategy to form continuous nanostructures with LiCl salts like spider webs around the inner walls of wood microchannels (i.e., fiber lumina). A single generator spontaneously produced a sustainable voltage of around 750 mV with a useful current of around 712 μA in ambient environment. And it also exhibited outstanding stability even when ambient humidity suddenly decreased to below 10% and stayed for 10 h. Besides, a connected system consisting of only six components outputted a voltage up to 4.40 V and current up to 4.16 mA, which can power LED lights. Our ionic wood shows promise for ambient moisture-energy conversion to develop the next self-sustained power system, with low-cost, sustainability and easily larger-scale productions.

1. Introduction

In pursuit of sustainable development, clean energy and biomaterials have attracted great attention in recent years [1,2]. Ambient moisture, a huge invisible blue energy residing in environment, has shown bright future in energy-conversion [3–5]. Recently, there has been that convert moisture energy into electricity under the mechanism such as redox reaction [6,7], streaming current [8–13] or ions gradient diffusion [14–30]. On this basis, great progress has been made in the research of energy harvesting directly from moisture in recent years. In one approach, it has been proved that electric power can be induced by ambient humidity gradient, which was always near a source of liquid water [8–13]. However, failure efficacy without liquid water source has constrained its scaling up and improvement of performance to some extent. In alternative strategy, direct energy harvesting from homogenous ambient has realized with the aid of gradient materials (such as g-GOF [14,16–18], g-PDA film [23] and a range of proteins [15]) which could build up an inner mobile ion concentration gradient when exposed to air [14–30]. Nevertheless, low output currents are a common pity in such spontaneous generators. It is even harder to get both satisfactory voltage and current for a single device. Besides, expensive raw materials and strict production processes are also obstacles to the future development of moisture power generation.

As an inexhaustible structural biomass material, natural wood consists of thousands of cellulose channels. Such well-ordered structures with highly anisotropic mechanical properties are mainly used for transporting ions and small molecules to maintain its living [31]. In terms of this, wood has been served creatively as ionic conductors to achieve energy conversion in recent years [32–37]. A kind of ion-conductive wood hydrogels inspired by muscle has been prepared successfully [37]. The characteristic of the hydrogel is the cross-linking network of aligned cellulose nanofibers and additive polyacrylamide polymer in wood microchannel [37]. Analogously, a synthesis method of anisotropic total cellulose wood aerogels by regenerating nanonetworks in wood microchannels after delignification was reported in 2020 [38]. Its anisotropic structure and exceptional specific surface areas made it possible as substrates for various purposes [38]. However, due to the removal of lignin, its relatively poor yield strength of 1.2 MPa, low Young's modulus of 25 ± 13 MP and high hydrophilia greatly impeded its use in the field of moisture power generation [38].

Inspired by predecessors, in this work, we have successfully made a novel aerogel wood without the removal of lignin. Compared with precedented wood aerogels, the aerogel woods prepared in this work not only possess substantial cellulose nanonetworks in wood microchannels

* Corresponding author.
E-mail address: dtliu@scut.edu.cn (D. Liu).

https://doi.org/10.1016/j.nanoen.2022.107065
Received 20 December 2021; Received in revised form 27 January 2022; Accepted 14 February 2022
Available online 17 February 2022

(Fig. 1a-I), but also have a surprising strength of Young's modulus up to 222 MP and yield strength up to 18 MP (Fig. S1 and Table S1). Besides, the stability of its structure also makes it an outstanding substrate for multifunctionalities, which makes up for the defects of traditional cellulose aerogels (Fig. S2a–e) and opens new opportunities for the development of aerogels.

Using aerogel woods as the substrates, via the synergy of freezing and salting out [39], a kind of ionic wood was developed from aerogel wood. In its retained intact top-down wood microchannels (i.e., fiber lumina), there are substantial continuous nanostructures modulated with ion providers (LiCl) like spiderwebs around the inner walls (Fig. 1a-II). Based on such sufficient mobile ions (Li^+) and continuous ionic bridges, we assembled a generator from ionic wood (Fig. 1a), which has achieved satisfactory moisture-induced power generation. A single generator can spontaneously produce a voltage up to 750 mV, and output a surprising current up to 712 μA. We compared the output current and voltage of our device with the exiting generators including liquid water-induced and moisture-induced (Fig. 1b). It was found that our single generator outputs a current with more than thousandfold increase and a competitive voltage than that of previously reported [14–30]. Besides, we also found that the generator could exhibit outstanding stability even when ambient humidity suddenly decreased

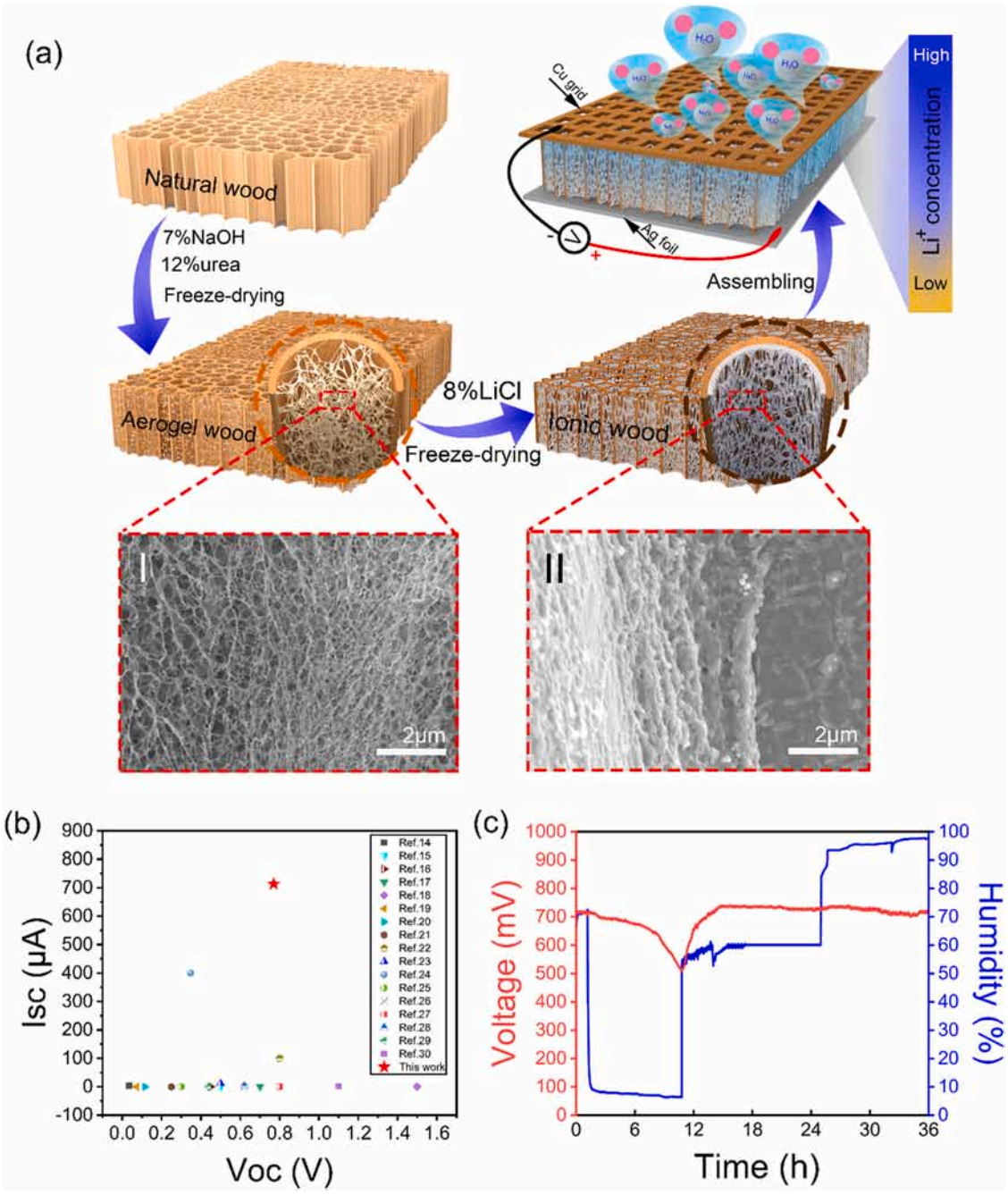

Fig. 1. Preparation of ionic wood and electricity generation of the generator. a) Schematic illustration of the preparation process of ionic wood and assembling of the generator. The existence of asymmetrical electrodes caused the difference of Li^+ ion concentration in ionic wood from top to bottom. I) SEM image of the 3D networks in the microchannel of aerogel wood. II) SEM image of "spider-web" in the microchannel of ionic wood. b) Comparison of the V_{oc} and I_{sc} of a single component with various single generators reported previously for water and moisture enabled generation. c) After the generator possessing a stable voltage, the responding of its voltage (red curve) to extreme humidity (blue curve) and drastic humidity changes, which proved the outstanding stability of our generator.

to below 10%, which has a certain energy storage effect (Fig. 1c). It shows a promising future for the applications of moisture power conversion.

2. Results and discussion

Herein, the generator was simply integrated by an ionic wood and two electrodes among which one is an open electrode (copper or silver grid) and another is an enclosed electrode (silver foil). Notably, ionic wood is the core of this design, and its whole preparation process is shown in Fig. 1a. Firstly, Balsa wood was treated with typical NaOH/Urea solution at − 13 °C for 24 h to partially dissolve the wood cell. The resulting sample was regenerated by 20 wt% tert-butly alcohol after it heating at 60 °C for 30 min, and the aerogel wood was then obtained after a freeze-drying process. Then, we directly immersed aerogel wood in 8 wt% LiCl solution overnight to ensure the sufficient covering of Li^+ and Cl^- onto cellulose nanonetworks. Crystal precipitation of LiCl around nanocellulose via − 60 °C freeze-drying turned the original three-dimensional (3D) cellulose nanonetworks (Fig. 1a-I) into two-dimensional (2D) spiderwebs-like structures, which modulated with ion providers (LiCl) and adhered to inner walls along the microchannels (Fig. 1a-II).

Encouragingly, the spontaneous hygroelectric generator from ambient air reported in this paper has shown both satisfactory voltage and current with a strong stability. Against ambient humidity fluctuation, we have studied its stability (Fig. 1c). For a generator that has been output steadily (voltage was about 710 mV) for 1 day, the voltage displayed almost no change by sharply decreasing humidity below 10%. When we continued to keep the extremely low humidity for 10 h, only a slight fluctuation was observed in latter experimental stage. However, the recovery of voltage to 738 mV was completed in only 2 h by enhancing humidity to normal 60% (Fig. 1c). Besides, we also found that the output voltage would not be damaged when we further suddenly boosted humidity above 90% and maintained this humidity condition for at least 8 h. Fundamentally, top-down 2D spiderweb-like structures tolerated the intermittent absence of external moisture, leading to the stable formation of continuous electrolyte while preserving water to avoid electrolytes leakage. In terms of power conversion, our generator is endowed a good energy storage, rendering continuous power output rather than the intermittent output reported in previous studies [12–14]. We also discussed the impacts of other environmental factors on the output (Fig. S7a and b). For example, the induced voltage was reduced by only about 30 mV after 2-hour heating of 42.2 °C. And when we stop the heating, the voltage was restored again because the LiCl was rehydrated (Fig. S7a). Additionally, facing the imposed stimuli of wind, the voltage output remained unchanged (Fig. S7b). Those results demonstrate that our generator can work with perfect stability in complex and changeable climatic environments.

To confirm ambient moisture as the origin of induced potential, we have tested the charging properties of our generators (4.0 cm × 4.0 cm × 0.5 cm) in four different humidity conditions (Fig. 2a) conducted in a homemade humidity cabinet (Fig. S3a and b). The generator from fresh ionic woods (completely dry) could produce voltage of around 700 mV whether at 90% or 60% ambient humidity in a time shorter than 10 h. More importantly, it shows distinctive ability for moisture-induced power generation at lower ambient humidity. For example, the fresh generator produced promising voltage output of 630 mV at very low ambient humidity of around 33% in 12 h. Under an extreme ambient

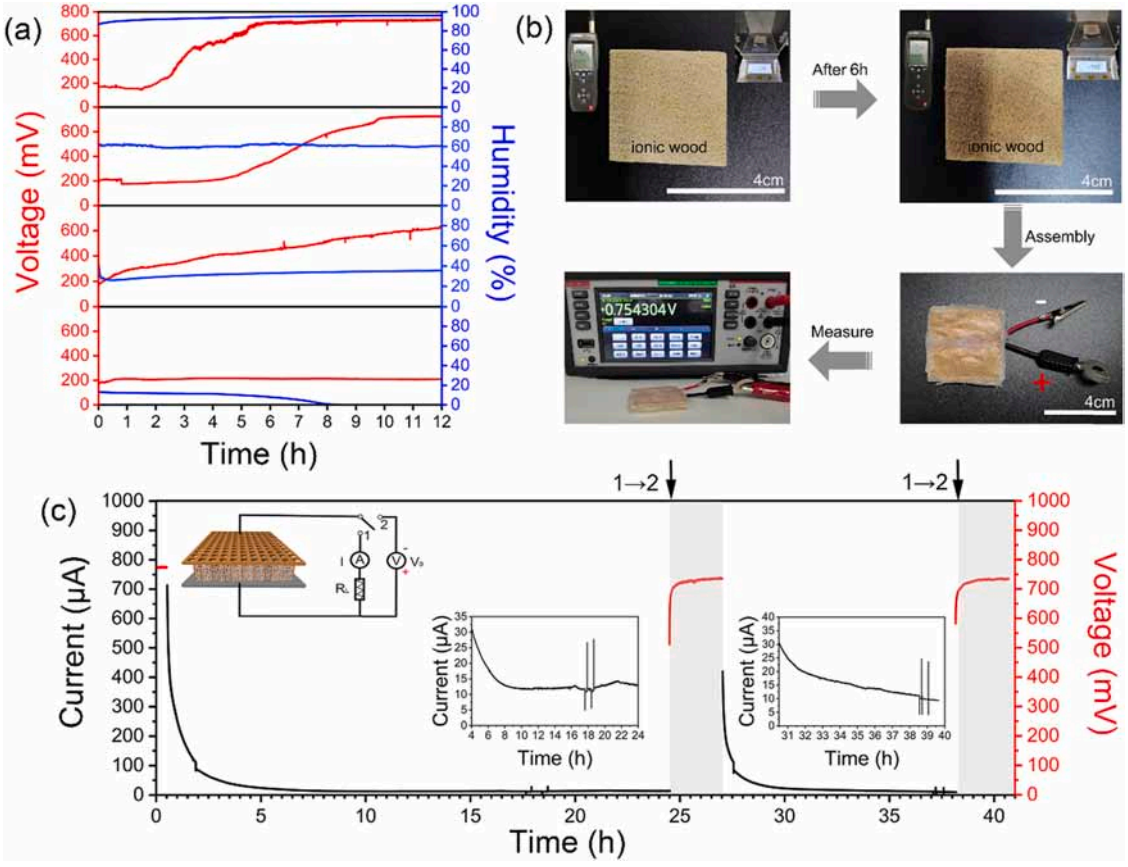

Fig. 2. a) The measured open-circuit voltages (V_{oc}s) (red curves) of the generators at different humidity (blue curves) of 0–14%, 27–47%, 59–62% and 86–96%, respectively. b) The whole macroscopic process of ionic wood from absorbing water to discharge in laboratory environment. c) The behavior of charging (V_{oc}, black curve) and discharging (I_{sc}, red curve) from a generator in the ambient moisture (at a relative humidity of about 60%). The inset shows the circuit diagram, in which connections to terminals 1 and 2 correspond to I_{sc} and V_{oc} measurements, respectively.

humidity lower than 10%, it still produced relatively high voltage of 210 mV and exhibited excellent stability even when the humidity decreased to 0%. The charging time for achieving the stable outputs prolonged with the decrease of ambient humidity, which proved the inducement of ambient humidity on the output performance of fresh generators.

Fig. 2b shows the macroscopic discharge process of our generator from ionic wood in a more specific way when exposed to air. We can see that the mass of a fresh ionic wood (4.0 cm × 4.0 cm × 0.3 cm) was 1.1834 g in the dry state, when the room temperature was 23.9 °C and relative humidity was 81.3%. Six hours later, the ionic wood was turned to 1.7988 g. At the time, the indoor temperature was 23.9 °C and the humidity was 83.4%. The water absorption of the ionic wood was 52% and a voltage of about 754 mV was generated. This means that only a small number of water molecules were required to generate such high output (Fig. 2b and Fig. S6a-c).

To evaluate the charge-discharge behaviors of our generator (4.0 cm × 4.0 cm × 0.3 cm), a cyclic V_{oc}-I_{sc} (open circuit voltage and short circuit current) test was performed at a constant ambient humidity around 60% (Fig. 2c). After the generator discharged continuously for 24 h, its V_{oc} only decreased from 770 mV to 512 mV with the reduction of I_{sc} from around 712μA to 13 μA. It is worthy to note that the voltage was rapidly restored to 720 mV at 60% humidity in a short time of 26 min, and further maintained at 733 ± 2 mV. At the same time, the current was gradually recovered to 418 μA after 4 h. The secondary discharge for continuous 12 h was performed, and the voltage was decreased to 583 mV while rapidly charged to 720 mV in 30 min. Another fascinating finding was that the lowest stable current output still retained a relative high level of around 10 μA, indicating their strong interaction with moisture in air (Fig. S6a-c).

The stable high electrical output of the device is mainly attributed to the "spider webs" in ionic wood. Compared with the cross section and axial section SEMs of natural wood (Fig. 3a), the substantial nanonetworks did form in aerogel wood with strong capillary force (Fig. 3b). That is why aerogel wood can work like huge pump to absorb the external liquid automatically and quickly under normal pressure. Fig. 3c shows the inner walls of the microchannels of ionic wood at different magnification levels. It is clear that the nanonetworks loading with plenty of LiCl particles, acting like "spider webs", adhere to luminas. On the one hand, the consecutive top-down "spider webs" served as a bridge for Li^+ ions migration, which is a vital condition for continuous electrolyte formation. On the other hand, due to the huge specific surface energy of nanonetworks, the "spider webs" has a strong water-holding ability, which is the precondition of stable output (Fig. 3g). To identify the superiority of this design, we compared the output voltage of ionic wood (Fig. 3g) with that of natural wood (Fig. 3d), natural wood doped with the same amount of LiCl (Natural wood + LiCl, Fig. 3e) and aerogel wood (Fig. 3f) at same humidity. Obviously, without the clever combination of the strongly hygroscopic LiCl salt and the "spider webs" structure, the resulting moisture-conversion voltages would be near-

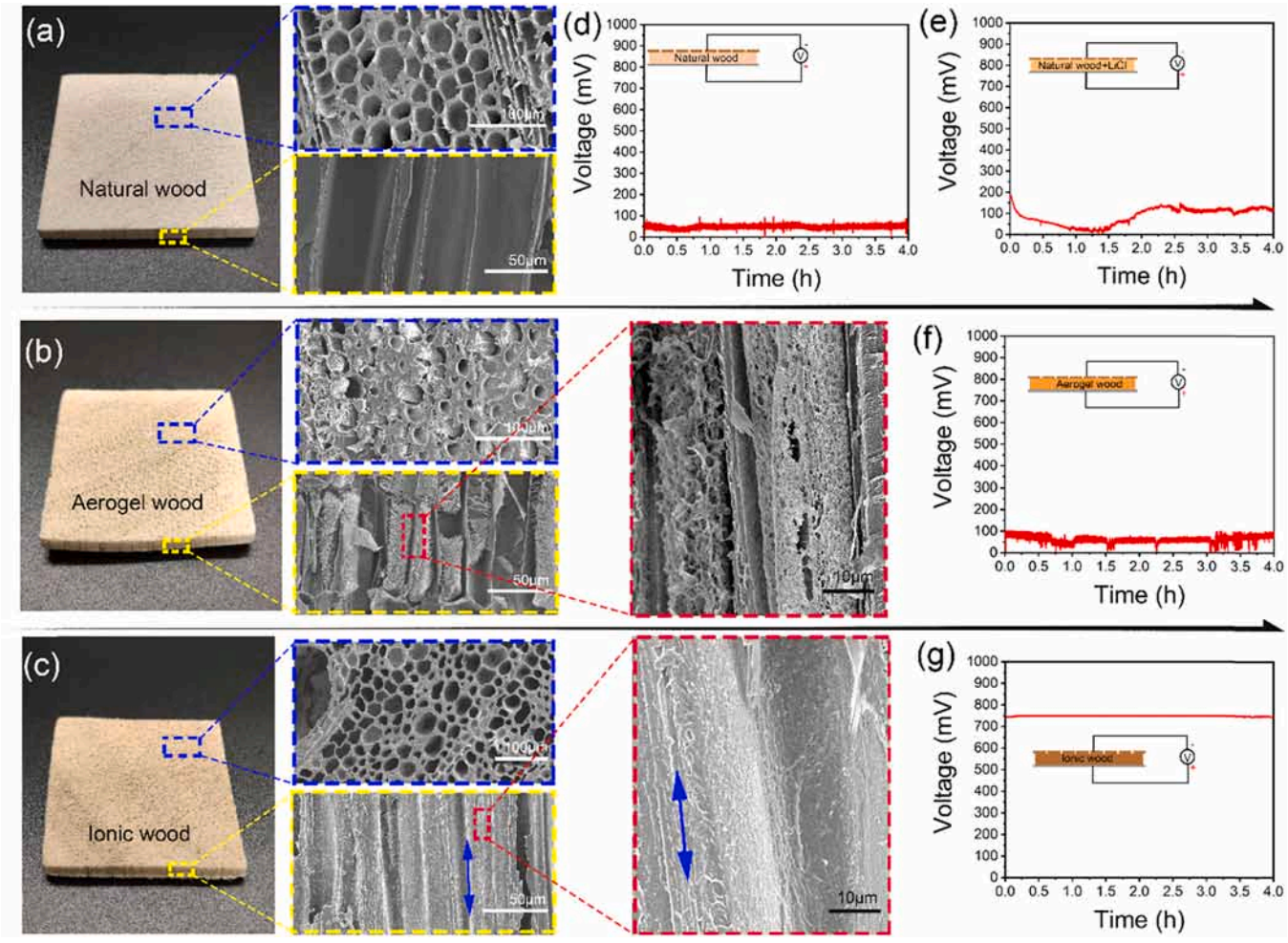

Fig. 3. Characterization of ionic wood successfully prepared and the demonstration of its successful application in moisture-induced generators. a) Optical photograph and SEM images of natural wood. b) and c) Optical photograph and SEM images of different sections of aerogel wood and ionic wood. d) The voltage output of natural wood at around 70% humidity. e) The voltage output of natural wood + LiCl (natural wood directly doped with 8% LiCl) at around 70% humidity. f) The voltage output of aerogel wood at around 70% humidity. g) The voltage output of ionic wood at around 70% humidity.

zero or very small.

For ionic wood, the specific spiderweb-like structure and ion provider (LiCl) contribute a perfect hygroscopic and water-holding ability, which are the precondition of high and stable output (Fig. 4a). LiCl is a highly hygroscopic salt and can spontaneously capture ambient moisture. Water molecules in air enter via the open Cu grid electrode (top side) while the alternative bottom side is sealed completely by Ag foil (Fig. 4b). In this way, a humidity gradient in the device will be built. When a fresh generator exposes to air, the anhydrous LiCl adjacent to Cu grid capture moisture and firstly liquefy to release free Li^+ ions, however, another side adjacent to the sealed silver foil is in reverse. With the help of the asymmetry of electrodes, there would build an ion concentration gradient. Finally, a built-in potential from bottom to top that opposes the direction of ion diffusion was established (Fig. 4b).

Once exposed to ambient air, anhydrous LiCl particles begin to combine with water molecules to form hydrating crystals and then continue to capture water until totally transforming into aqueous salt solution (i.e., electrolyte) where they could still interact with ambient moisture (Fig. 4c and S6a). In a 12-day monitoring, we found that the mass of ionic wood reached the maximum value after about 20 h and then still fluctuated along with the changes of ambient humidity (Fig. S6a). Such dynamic interaction is an important evidence that the device can sustainably generate electricity from moisture in air over time (Fig. S6b and c). Hence, the moisture-induced mechanism of our generator is based on the concept of self-formation and self-diffusion of continuous electrolytes in top-down constrained microchannels (Fig. 4c).

After dissolving and regenerating processes, the microchannels of aerogel wood had a zeta potential of around -60 ± 6 mV compared with -27 ± 3 mV of natural wood. So much low zeta potential of aerogel wood indicates a higher negative charge density of the inner walls of ionic wood. Based on double electric layer (EDL) theory [40–43], a surface-charge-governed ion transport is driven along the spiderweb-like structure (Fig. 4c). Against an immobile Cl^- and -O- anionic background, mobile Li^+ ions diffuse from top to bottom. The nanofluidic effect [44–49] indicates that the electrostatic field surrounding spiderweb-like networks in microchannels actively drags counter-ions to migrate, but effectively ignores co-ions. Moreover, there is a stronger steric hindrance for Cl^- due to its larger radius. Therefore, most of Cl^- ions retain with thermal motion in small regions due to the bondage of spiderweb-like structures when electrolytes diffuse across the microchannels. According to the nanofluidic ion transport effect [44–49], Li^+ ions would migrate along the spider-like networks (Fig. 4c). As a result, an ion concentration gradient will be built across the device.

To verify this speculation, the investigations of Li^+ and Cl^- ions distribution on top and bottom sides of ionic wood were characterized by XPS (Fig. 4d and S5). The sample of 2# simulated the state (one open

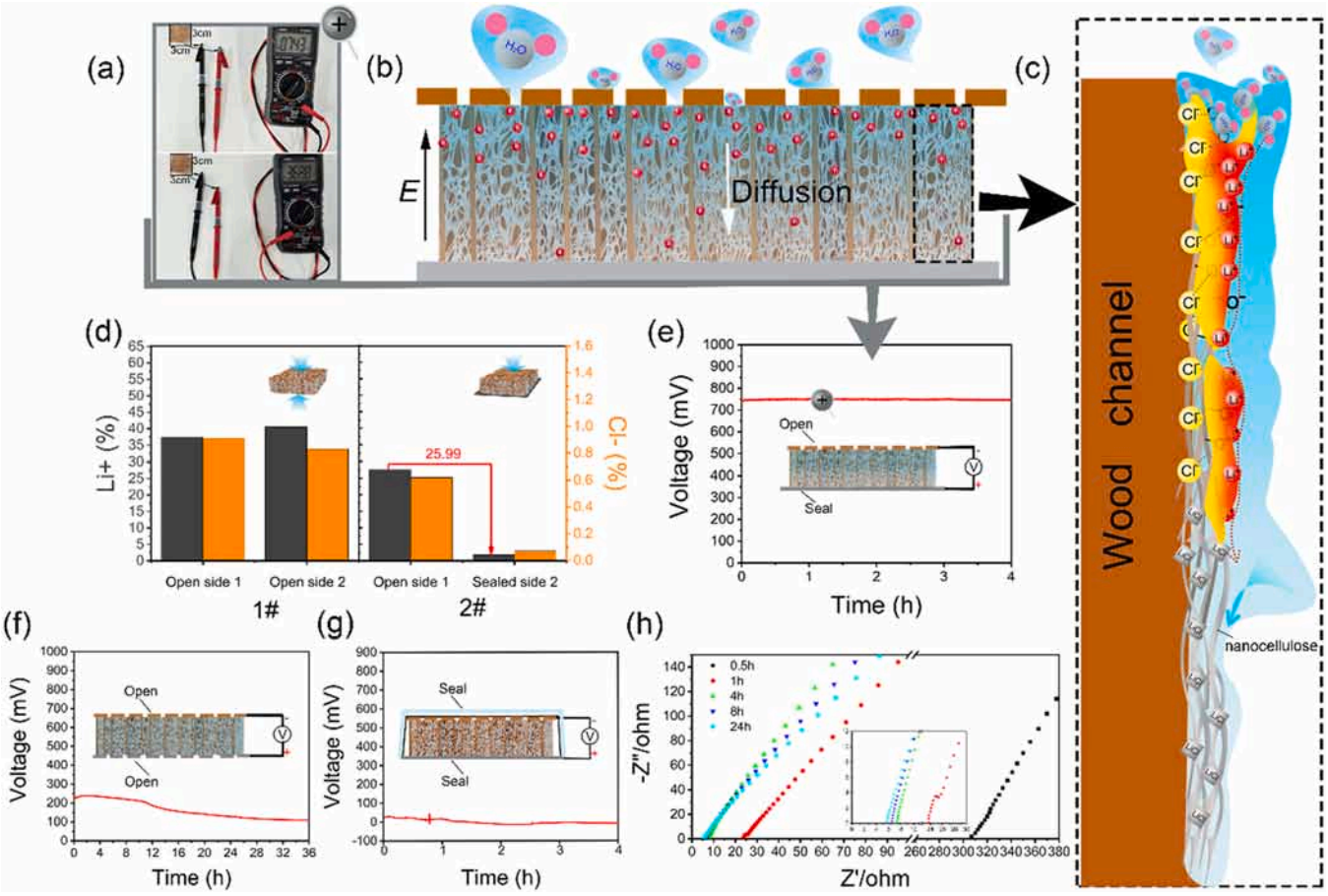

Fig. 4. Mechanism of the power generation. a) Photographs of the measurements of the V_{oc} (top) and I_{sc} (bottom) from a 3.0 cm × 3.0 cm × 0.3 cm generator. b) The front view of the schematic diagram of moisture-dependent power generation of the device. c) Anatomic diagram of a microchannel in ionic wood. The detailed diagram shows the formation of ionization gradient under the induction of humidity gradient (represented by the blue background). Anhydrous LiCl particles (gray square) residing in ionic wood-channel "spider webs" would gradually liquefy (represented by the red and yellow background) and separate Li^+ ions (red balls) and Cl^- ions (yellow balls) under the induction of humidity gradient. d) The corresponding Li^+ and Cl^- contents of 1# and 2# in their different surfaces from XPS results. e) The 4 h recording of V_{oc} from a generator using Cu grid as open electrode and Ag foil as sealed electrode. f) The 36 h recording of V_{oc} from a generator using Cu grid as open electrode and Ag grid as sealed electrode. g) The 4 h recording of V_{oc} from a generator (using Cu grid as open electrode and Ag foil as sealed electrode) in a completely sealed state. h) EIS curves of a 4.0 cm × 4.0 cm × 0.3 cm fresh ionic wood according to its exposure time under a room humidity of around 70%.

side and another sealed side) of the top and bottom surfaces of the ionic wood while the generator was normally operating (Fig. 4d). For comparison, sample of 1# were open on both sides (Fig. 4d). After been for 12 h at ambient humidity of 60 ± 5%, we can see that the distribution of Cl^- shows few differences in both sides of 1# and 2#, which are all less than 1%. Nevertheless, for 2#, the open side displays a higher 25.99% in Li^+ content than the sealed side while there is almost no change for 1#. Therefore, the asymmetrical electrodes assembled on the generator did help to construct an ion concentration gradient.

In order to demonstrate the important roles of moisture and moisture gradient in power generation, more investigations were carried out. In Fig. 4e, the generator produced a stable voltage of around 740 mV by the open electrode exposed to ambient air. While there was a near-zero voltage shown in Fig. 4g when sealed the open electrode of the generator with a polyethylene film. Such observations provide the evidence that the output of our device is mainly induced by ambient moisture. Following, the influence of moisture gradient on power generation was also investigated (Fig. 4f). It is observed that the device with two open electrodes did not generate a high output voltage as seen in Fig. 2a under the same 60% humidity. And the trend of voltage rising firstly and then falling later indicates that humidity gradient is the key for high output even though water molecules are the source of power.

Then, to evaluate the influence of exposure time on nanofluidic ion-transport behavior, the ionic conductivity of ionic wood was measured by electro-chemical impedance spectroscopy (EIS, Fig. 4h) where the lowest points on the real axis correspond to ionic resistances. With the increase of exposure time, ionic wood captured more water molecules leading to more release of Li^+ ions and decreasing resistance of ion movement, as evinced in Fig. 4h. Moreover, the experimental results show that ionic resistances decreased below 10 ohms after 4 h exposure time.

In further experimental works, we investigated the effects of thickness of ionic wood on the outputs. By maintaining the same cross-sectional areas of ionic woods with around 16.0 cm^2

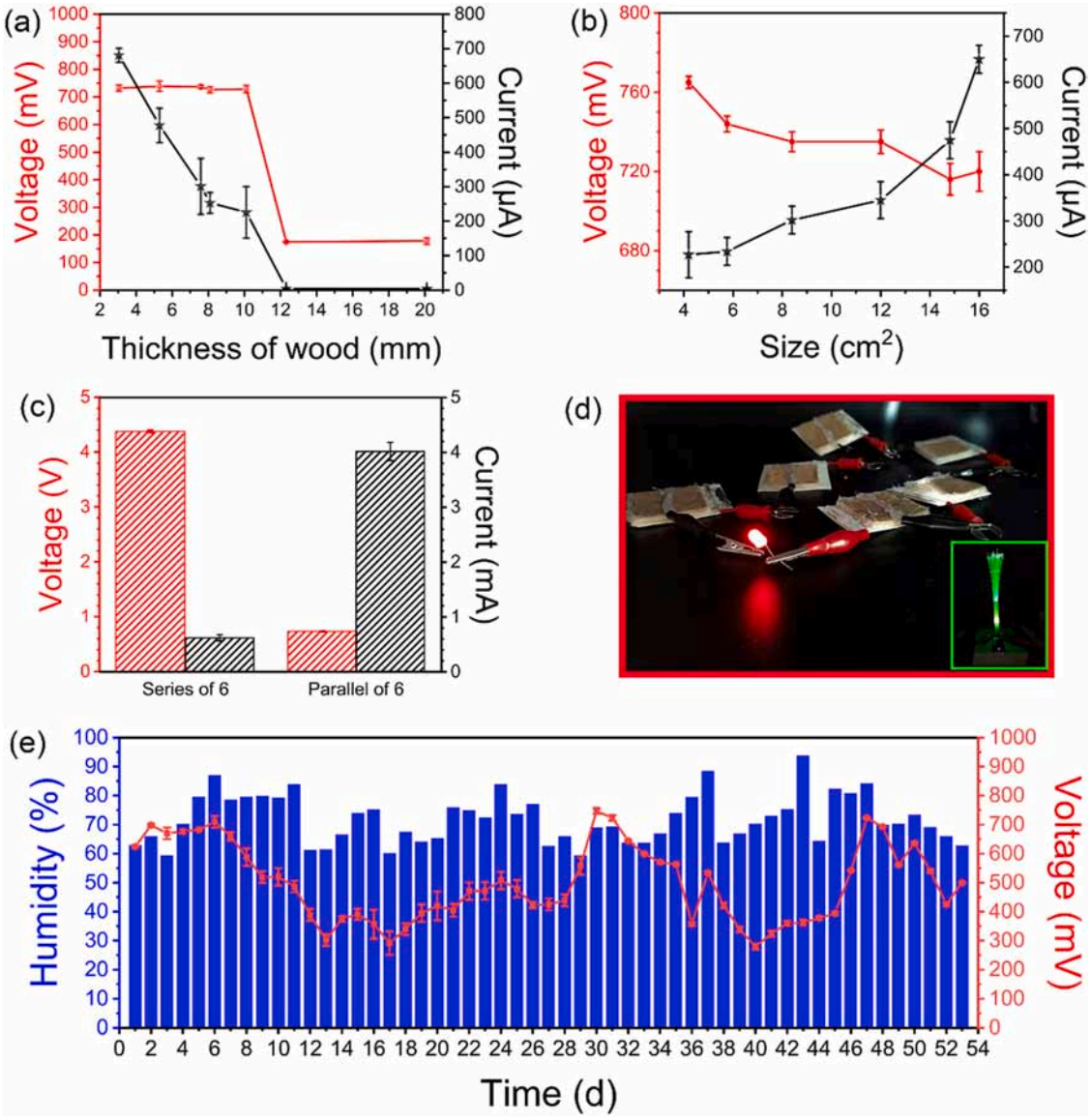

Fig. 5. Scaling and applications of the moisture-induced electricity. a) V_{oc} (red) and I_{sc} (black) plotted against device thickness at an ambient relative humidity of about 60%, for an ionic wood size of 4.0 cm × 4.0 cm. b) V_{oc} (red) and I_{sc} (black) plotted against device size at an ambient relative humidity of about 60%, for an ionic wood thickness of roughly 0.3 cm. c) V_{oc} (red) and I_{sc} (black) obtained by connecting six components in series and in parallel, respectively. d) photographs of two LEDs (red and green) were driven respectively by six components (4.0 cm × 4.0 cm × 0.3 cm, the thickness error range is within 0.1 cm) connected in series. And Each of the generators was fabricated in the same way as shown in Fig. 1a. e) A long-term recording of the voltages (red curve) from a generator for about 53 days. The ambient relative humidity (blue bar) was also recorded.

(4.0 cm × 4.0 cm), the obtained devices generated unsatisfactory current and voltage when the thicknesses increased more than 12.0 cm (Fig. 5a). However, the devices with thickness from 0.3 cm to 1.0 cm produced stable voltage around 730 mV but showed a gradually decreased current tendency. The performance degradation of the devices may have something to do with the distance of ion transport. The ionic wood is thicker, the path of ion transport is longer. An extensive analysis points out that the devices from ionic woods with around 0.3 cm thickness generate perfect voltage and current. That is why the thickness of 0.3 cm served as the standard of following studies.

Considering in a micro perspective, an ionic wood can be viewed roughly as a matrix integrated by a number of top-down microchannels in parallel. Every microchannel can be simulated as a nanogenerator. For a generator from ionic wood, we have a well-grounded imagination that it is made up of thousands of nanogenerators connected in parallel. In Fig. 5b, the relationship between the sizes of ionic woods and their electric outputs have proved the rationality of above assumption. It is obvious that at the same thickness of 0.3 cm, the output currents of 4.2 cm^2, 5.8 cm^2, 8.4 cm^2, 12.0 cm^2, 14.8 cm^2 and 16.0 cm^2 generators are 227 ± 50 μA, 234 ± 30 μA, 302 ± 30 μA, 345 ± 40 μA, 475 ± 40 μA and 650 ± 30 μA, respectively, while their output voltages are not much difference. Obviously, such phenomenon conforms to the law of voltage and current in series and parallel circuits and reveals that the current value of a generator would increase as its cross-section size increased. Therefore, its current can be easily scaled up by simply expanding the size of ionic wood. In this way, we have achieved exceptional current values of about 700 μA employing ionic woods with 4.0 cm × 4.0 cm × 0.3 cm.

Besides, we can also get a larger output through simply connecting devices in series or parallel. In Fig. 5c we have got one V_{oc} up to 4.40 V in series of 6 generators and one I_{sc} up to 4.16 mA in parallel of 6 generators. And they have been easy to power two LED lights (green and red, Fig. 5d). In Fig. 5e, we display a long-term recording of V_{oc} (red curve) of a generator for about 53 days in the laboratory environment, which further indicates the huge potential for practical application of our generator.

From the FT-IR map of natural wood, aerogel wood and ionic wood (Fig. S4a), such message that there is no new absorption peak appeared is delivered. This indicates that no new groups were introduced into cellulose macromolecules in the preparation of aerogel wood and ionic wood. Compared with natural wood, the disappearance of absorption peak of aerogel wood and ionic wood at around 1720 cm^{-1} was mainly due to the dissolution of part hemicellulose. It was further proved that there were no new functional groups on the regenerated nanonetworks. For aerogel wood and ionic wood, the functional groups on them are just a lot more hydroxyl groups than natural wood. Therefore, the influence of other functional groups on power generation was eliminated. In Fig. S4b, compared with the intensity of crystalline native cellulose I (14.7°, 16.5°, 22.5°, and 34.5°), intensity decreases and disappearances of aerogel wood indicates the dissolution/regeneration of cellulose. While the increase intensity of ionic wood may be caused by LiCl crystal. The reduction of intensity in 14.7° and a broader amorphous peak (21.5) for aerogel wood demonstrate more generation of amorphous cellulose, a further indication of partial dissolution/regeneration mechanism.

The importance of wood channel directions was also discussed in next (Fig. S8). Take two identical ionic woods (4.0 cm × 4.0 cm × 0.3 cm) named 3# and 4#, in which 3# connected the electrodes in its vertical direction and 4# connected the electrodes in its horizontal direction as shown in Fig. S8. Apparently, for 3#, the current and voltage values are much better than for 4#. As to 4#, Li^+ ions would travel in a predetermined direction without reaching its two electrodes. However, in 3#, two electrodes were installed in the both ends of microchannels, where Li^+ can not only transport rapidly along the channels under the driving of humidity gradient but also reach both ends to touch the electrodes and inspire a potential under the effect of EDL [40–43]. Therefore, in the absence of straight continuous ions flow, 4# exhibits a poor voltage and current of about 180 mV and 3 μA, which are far from the output performance of 3#.

During the preparation of ionic wood, the concentration of LiCl solution has a certain influence on the energy conversion (Fig. S9a). Six aerogel woods in a same size (2.0 cm × 2.0 cm × 0.3 cm) were respectively soaking into 3 wt%, 5 wt%, 8 wt%, 11 wt%, 15 wt% and 20 wt% LiCl solutions (20 mL) to obtain a group of ionic woods with different contents of LiCl after freeze drying. Before testing, the devices from above ionic woods were left overnight at around 70% humidity. The weight of adsorbed moisture divided by the total ionic wood weight was named as W_{H2O}. As predicted, the W_{H2O} increased with the increase of LiCl concentration. However, the V_{oc} and I_{sc} of corresponding devices were not in the same rhythm with W_{H2O}. Apparently, the devices from ionic woods treated by 8 wt% LiCl solution yielded the highest voltage and current and there would be unfulfilling outputs when the concentrations are more than 10 wt%. For ionic woods treated with higher LiCl concentration, there would be more LiCl particles filled in the microchannels occupying the space for ion movement and the nanofluidic effect was also destroyed. Therefore, in Fig. S9a, the devices from ionic woods treated by 20 wt% LiCl solution only have 300–400 mV V_{oc} and 19–20 μA I_{sc}.

In Table S2, there is a set of simple records of LiCl load of ten 2.0 cm × 2.0 cm × 0.3 cm ionic woods that were treated with 20 mL 8 wt% LiCl respectively. We can know roughly that an ionic wood in this size (2.0 cm × 2.0 cm × 0.3 cm) has a LiCl load of about 17 wt%. It is also found that a small range of ion load fluctuation did not affect the outputs of the devices through electrical tests (Fig. S9b). Besides, surprisingly, the outputs of a device from 8 wt% $CaCl_2$-doped ionic wood can also reach around 730 mV in ambient air, which further indicates the diversity and universality of our ionic wood (Fig. S10).

To make our conclusions more convincing, a series of controlled experiments for asymmetric electrodes were conducted. Firstly, for a fresh device employing Ag grid as the open electrode and Ag foil as the closed electrode, its charging behavior was similar as the generator sandwiched by Cu grid and Ag foil (Fig. S11). Besides, when the open electrode was changed from Ag grid to Cu grid, its output voltage, after being stable, would eventually remain around 800 mV (Fig. S12). Now the influence of different electrode materials on the induced outputs was excluded and thus the importance of electrode shape was highlighted. As to a generator with a stable humidity gradient, there would be a suddenly voltage drop from around 770 mV to around 632 mV when the equilibrium got damaged deliberately by replacing the Ag foil with an Ag grid (Fig. S13). Benefiting the energy storage effect of ionic wood, the voltage has not changed much.

3. Conclusions

We have employed the sufficient mobile Li^+ ions along continuous top-down nanostructures transport phenomenon of ionic wood fabricated via a facile chemical treatment of natural wood. A single generator from ionic wood offered both satisfactory voltage and current of up to 750 mV and 712 μA without any external auxiliaries. It exhibits high stability at ultralow humidity (< 10%) and exceeds the performance of most current hygroelectric generators. Such ability implies a huge potential of our device in the application of extremely dry environment. Simply expanding the size of ionic wood or connecting them in series or in parallel, a higher output could be easily achieved, which has the potential to power many common electronic devices and to break the barrier for moisture-induced generators from laboratory to life. Our work provides a new possibility for the application of abundantly available wood for low-grade water energy harvesting and opens up a new scope towards the development of green and spontaneous power-supply devices.

4. Experimental methods

4.1. Materials and chemicals

The natural woods were cut perpendicular to the growth direction of the Balsa wood. Sodium hydroxide (NaOH) and urea (both purchased from Tianjin Damao Chemical Reagent Factory) were used for in situ dissolution of cellulose. Tert-butyl alcohol (came from Tianjin Damao Chemical Reagent Factory) was used for solidification of nanocellulose networks. lithium chloride (LiCl) was also bought from Tianjin Damao Chemical Reagent Factory.

4.2. Preparation of aerogel wood

Balsa wood (4.0 cm × 4.0 cm × 0.3 cm) was wash with ultrasound in 90 wt% ethanol for 20 min and then it was transferred to fume hood for 2 h to dry. At room temperature, the dry wood block was firstly immersed into a solution containing 7 wt% sodium hydroxide and 12 wt % urea for 30 min until it was fully infiltrated with the alkaline salt solution. Subsequently, the whole solution containing the wood was frozen at − 13 °C for 24 h before being taken out and placed at 60 °C for 30 min. Then, the treated sample was introduced into a 20 wt% tert-butly alcohol solvent to exchange, which was repeated four times. The resultant sample was frozen in − 40 °C, followed by freeze-drying (−60 °C) for at least 12 h to yield aerogel wood.

4.3. Preparation of ionic wood and fabrication of the generator

The aerogel wood was immersed in 20 mL 8 wt% LiCl solution for about 12 h and subsequently freeze-drying to obtain the ionic wood. Before freeze-drying, the sample was placed in − 60 °C for 4 h. The fabrication of the generator is rather simple. To fabricate a generator, the ionic wood only needs to be sandwiched between a silver (Ag) sheet and a silver (Ag)/copper (Cu) grid that are of equal size as ionic wood. Emphatically, the generators would be stored in a vacuum seal on one or both sides prior to a series of testing in case of the effects of moisture in the air as much as possible.

4.4. Characterization

Morphologies of natural wood, aerogel wood and ionic wood were analyzed using a field emission scanning electron microscope (Hitachi SU5000, Japan). Nicolet IS50 - Nicolet Continuum (Thermo Fisher Scientific) was used to discover whether there were new functional groups in aerogel wood. XRD was performed by multi-position automatic injection X-ray diffractometer (X′pert Powder, Japan). The scans were performed over 2θ of 5–40° with a step size of 0.0131°. XPS was performed by Thermo Scientific K-Alpha from America. EIS measurement was carried out by a CHI lectrochemical workstation and was performed with a 50 mV AC amplitude in the frequency range of 0.01 Hz to 106 MHz. The zeta potentials of natural wood and aerogel wood were measured using a solid surface Zeta potential tester (SurPASS 3, Austria) by flow potential method at pH = 7. The compressive strengths of natural wood, aerogel wood and ionic wood were evaluated through longitudinal compression in an Instron 5982, utilizing a 20 kN load cell at a strain rate of 10%/min. The output voltage and current were recorded by digital multimeters (ZTY890D and Keithley DMM6500). Humidity change using temperature and humidity meter CEM DT8896 recorded. Humidity control was conducted in a homemade humidity cabinet.

CRediT authorship contribution statement

Yang Li: Investigation, Visualization, Writing – original draft. **Jiedong Cui:** Validation. **Haoyu Shen:** Formal analysis. **Chaocheng Liu:** Software. **Peilin Wu:** Data curation. **Zhiyun Qian:** Resources. **Yulong Duan:** Methodology. **Detao Liu:** Conceptualization, Supervision, Project administration, Funding acquisition, Writing – review & editing.

Declaration of Competing Interest

The authors declare the following financial interests/personal relationships which may be considered as potential competing interests: Detao Liu reports financial support was provided by South China University of Technology. Detao Liu reports a relationship with Guangdong Basic and Applied Basic Research Foundation of Guangdong Province that includes: funding grants. Detao Liu reports a relationship with Science and Technology Planning Project of Guangdong Province that includes: funding grants.

Acknowledgement

This work was kindly supported by Guangdong Basic and Applied Basic Research Foundation of Guangdong Province (No. 2020A1515011013) and Science and Technology Planning Project of Guangdong Province (No. 2020A050515004).

Appendix A. Supporting information

Supplementary data associated with this article can be found in the online version at doi:10.1016/j.nanoen.2022.107065.

References

[1] S. Chu, A. Majumdar, Opportunities and challenges for a sustainable energy future, Nature 488 (2012) 294–303.
[2] Z. Zhang, X. Li, J. Yin, Y. Xu, W. Fei, M. Xue, Q. Wang, J. Zhou, W. Guo, Emerging hydrovoltaic technology, Nat. Nanotechnol. 13 (2018) 1109–1119.
[3] D. Shen, W.W. Duley, P. Peng, M. Xiao, J. Feng, L. Liu, G. Zou, Y. Zhou, Moisture-enabled electricity generation: from physics and materials to self-powered applications, Adv. Mater. 32 (2020), 2003722.
[4] V. Dao, N.H. Vu, H.T. Dang, S. Yun, Recent advances and challenges for water evaporation-induced electricity toward applications, Nano Energy 85 (2021) 2211–2855.
[5] S.B. Pandya, H.R. Jariwala, Single- and multiobjective optimal power flow with stochastic wind and solar power plants using moth flame optimization algorithm, Smart Sci. 5 (2021) 1–30.
[6] X. Zhang, J. Yang, R. Borayek, H. Qu, D.K. Nandakumar, Q. Zhang, J. Ding, S. C. Tan, Super-hygroscopic film for wearables with dual functions of expediting sweat evaporation and energy harvesting, Nano Energy 75 (2020), 104873.
[7] Y. Wang, M. Dai, H. Wu, L. Xu, T. Zhang, W. Chen, Z.L. Wang, Y. Yang, Waterproof, breathable and washable triboelectric nanogenerator based on electrospun nanofiber films for wearable electronics, Nano Energy 90 (2021) 2211–2855.
[8] S. Zhang, W. Chu, L. Li, W. Guo, Voltage distribution in porous carbon black films induced by water evaporation, J. Phys. Chem. C 125 (2021) 8959–8964.
[9] T. Tabrizizadeh, J. Wang, R. Kumar, S. Chaurasia, K. Stamplecoskie, G. Liu, Water-evaporation-induced electric generator built from carbonized electrospun polyacrylonitrile nanofiber mats, ACS Appl. Mater. Interfaces 13 (2021) 50900–50910.
[10] R. Zhang, S. Wang, M.-H. Yeh, C. Pan, L. Lin, R. Yu, Y. Zhang, L. Zheng, Z. Jiao, Z. L. Wang, A streaming potential/current-based microfluidic direct current generator for self-powered nanosystems, Adv. Mater. 27 (2015) 6482–6487.
[11] G. Xue, Y. Xu, T. Ding, J. Li, J. Yin, W. Fei, Y. Cao, J. Yu, L. Yuan, L. Gong, J. Chen, S. Deng, J. Zhou, W. Guo, Water-evaporation-induced electricity with nanostructured carbon materials, Nat. Nanotechnol. 12 (2017) 317–321.
[12] J. Li, K. Liu, G. Xue, T. Ding, P. Yang, Q. Chen, Y. Shen, S. Li, G. Feng, A. Shen, M. Xu, J. Zhou, Electricity generation from water droplets via capillary infiltrating, Nano Energy 48 (2018) 211–216.
[13] X. Zhou, W. Zhang, C. Zhang, Y. Tan, J. Guo, Z. Sun, X. Deng, Harvesting electricity from water evaporation through microchannels of natural wood, ACS Appl. Mater. Interfaces 12 (2020) 11232–11239.
[14] F. Zhao, H. Cheng, Z. Zhang, L. Jiang, L. Qu, Direct power generation from a graphene oxide film under moisture, Adv. Mater. 27 (2015) 4351–4357.
[15] X. Liu, H. Gao, J.E. Ward, X. Liu, B. Yin, T. Fu, J. Chen, D.R. Lovley, J. Yao, Power generation from ambient humidity using protein nanowires, Nature 578 (2020) 550–554.
[16] H. Cheng, Y. Huang, F. Zhao, C. Yang, P. Zhang, L. Jiang, G. Shi, L. Qu, Spontaneous power source in ambient air of a well-directionally reduced graphene oxide bulk, Energy Environ. Sci. 11 (2018) 2839–2845.
[17] Y. Liang, F. Zhao, Z. Cheng, Y. Deng, Y. Xiao, H. Cheng, P. Zhang, Y. Huang, H. Shao, L. Qu, Electric power generationviaasymmetric moisturizing of graphene oxide for flexible, printable and portable electronics, Energy Environ. Sci. 11 (2018) 1730–1735.

[18] Y. Huang, H. Cheng, C. Yang, P. Zhang, Q. Liao, H. Yao, G. Shi, L. Qu, Interface-mediated hygroelectric generator with an output voltage approaching 1.5 volts, Nat. Commun. 9 (2018) 4166.
[19] X. Nie, B. Ji, N. Chen, L. Yuan, Q. Han, L. Qu, Gradient doped polymer nanowire for moistelectric nanogenerator, Nano Energy 46 (2018) 297–304.
[20] W. Yang, X. Li, X. Han, W. Zhang, C. Li, Asymmetric ionic aerogel of biologic nanofibrils for harvesting electricity from moisture, Nano Energy 71 (2020), 104610.
[21] X. Gao, T. Xu, C. Shao, Y. Han, B. Lu, Z. Zhang, L. Qu, Electric power generation using paper materials, J. Mater. Chem. A 7 (2019) 20574–20578.
[22] T. Xu, X. Ding, Y. Huang, C. Shao, L. Song, X. Gao, Z. Zhang, L. Qu, Type 2 diabetes mellitus is associated with increased left ventricular mass independent of coronary artery volume, Energy Environ. Sci.. 12 (2019) 972–978.
[23] L. Li, Z. Chen, M. Hao, S. Wang, T. Zhang, Moisture-driven power generation for multifunctional flexible sensing systems, Nano Lett. 19 (2019) 5544–5552.
[24] Z. Luo, C. Liu, S. Fan, A moisture induced self-charging device for energy harvesting and storage, Nano Energy 60 (2019) 371–376.
[25] G. Ren, Z. Wang, B. Zhang, X. Liu, J. Ye, Q. Hu, S. Zhou, A facile and sustainable hygroelectric generator using whole-cell Geobacter sulfurreducens, Nano Energy 89 (2021) 2211–2855.
[26] J. Eun, S. Jeon, Direct fabrication of high performance moisture-driven power generators using laser induced graphitization of sodium chloride-impregnated cellulose nanofiber films, Nano Energy 92 (2022) 2211–2855.
[27] Z. Sun, L. Feng, C. Xiong, X. He, L. Wang, X. Qin, J. Yu, Electrospun nanofiber fabric: an efficient, breathable and wearable moist-electric generator, J. Mater. Chem. A 9 (2021) 7085–7093.
[28] K. Gao, J. Sun, X. Lin, Y. Li, X. Sun, N. Chen, L. Qu, High-performance flexible and integratable MEG devices from sulfonated carbon solid acids containing strong Brønsted acid sites, J. Mater. Chem. A 9 (2021) 24488–24494.
[29] K.H. Lee, D.J. Kang, W. Eom, H. Lee, T.H. Han, Activating γ-graphyne nanoribbons as bifunctional electrocatalysts toward oxygen reduction and hydrogen evolution reactions by edge termination and nitrogen doping, Chem. Eng. J. 430 (2022) 1385–8947.
[30] Z. Sun, L. Feng, X. Wen, L. Wang, X. Qin, J. Yu, Nanofiber fabric based ion-gradient-enhanced moist-electric generator with a sustained voltage output of 1.1 volts, Mater. Horiz. 8 (2021) 2303–2309.
[31] H. Zhu, W. Luo, P.N. Ciesielski, Z. Fang, J. Zhu, G. Henriksson, M.E. Himmel, L. Hu, Wood-derived materials for green electronics, biological devices, and energy applications, Chem. Rev. 116 (2016) 9305–9374.
[32] G. Chen, T. Li, C. Chen, C. Wang, Y. Liu, W. Kong, D. Liu, B. Jiang, S. He, Y. Kuang, L. Hu, A highly conductive cationic wood membrane, Adv. Funct. Mater. 29 (2019), 1902772.
[33] C. Chen, J. Song, J. Cheng, Z. Pang, L. Hu, Highly elastic hydrated cellulosic materials with durable compressibility and tunable conductivity, ACS Nano 14 (2020) 16723–16734.
[34] T. Li, X. Zhang, S.D. Lacey, R. Mi, X. Zhao, F. Jiang, J. Song, Z. Liu, G. Chen, J. Dai, Y. Yao, S. Das, R. Yang, R.M. B, L. Hu, Cellulose ionic conductors with high differential thermal voltage for low-grade heat harvesting, Nat. Mater. 18 (2019) 608–613.
[35] Y. Yang, X. Sun, Z. Cheng, A. Mukhopadhyay, A. Natan, C. Liu, D. Cao, H. Zhu, Retarding Ostwald ripening to directly cast 3D porous graphene oxide bulks at open ambient conditions, ACS Appl. Energy Mater. 3 (2020) 6249–6257.
[36] J. Sun, H. Guo, G.N. Schadli, K. Tu, S. Schar, F.W.M.R. Schwarze, Sci. Adv. 7 (2021) eabd9138.
[37] W. Kong, C. Wang, C. Jia, Y. Kuang, G. Pastel, C. Chen, G. Chen, S. He, H. Huang, J. Zhang, S. Wang, L. Hu, Muscle-inspired highly anisotropic, strong, ion-conductive hydrogels, Adv. Mater. 30 (2018), 1801934.
[38] J. Garemark, X. Yang, X. Sheng, O. Cheung, L. Sun, L. Berglund, Y. Li, Top-down approach making anisotropic cellulose aerogels as universal substrates for multifunctionalization, ACS Nano 14 (2020) 7111–7120.
[39] M. Hua, S. Wu, Y. Ma, Y. Zhao, X. He, Strong tough hydrogels via the synergy of freeze-casting and salting out, Nature 590 (2021) 594–599.
[40] L. Joly, C. Ybert, E. Trizac, L. Bocquet, Hydrodynamics within the electric double layer on slipping surfaces, Phys. Rev. Lett. 93 (2004), 257805, 257805-257805.
[41] M.Z. Bazant, B.D. Storey, A.A. Kornyshev, Erratum: double layer in ionic liquids: overscreening versus crowding [Phys. Rev. Lett.106, 046102 (2011), Phys. Rev. Lett. 109 (2012), 149903.
[42] A. Fruchtman, Electric field in a double layer and the imparted momentum, Phys. Rev. Lett. 96 (2006), 065002.
[43] R. Yamamoto, H. Morisaki, O. Sakata, H. Shimotani, H. Yuan, Y. Iwasa, T. Kimura, Y. Wakabayashi, External electric field dependence of the structure of the electric double layer at an ionic liquid/Au interface, Appl. Phys. Lett. 101 (2012), 053122.
[44] T. Li, S.X. Li, W. Kong, C. Chen, E. Hitz, C. Jia, J. Dai, X. Zhang, R. Briber, Z. Siwy, M. Reed, L. Hu, A nanofluidic ion regulation membrane with aligned cellulose nanofibers, Sci. Adv. 5 (2019) eaau4238.
[45] W. Sparreboom, A. Van den Berg, J.C.T. Eijkel, Principles and applications of nanofluidic transport, Nat. Nanotechnol. 4 (2009) 713–720.
[46] C. Duan, A. Majumdar, Anomalous ion transport in 2-nm hydrophilic nanochannels, Nat. Nanotechnol. 5 (2010) 848–852.
[47] M. Wang, H. Meng, D. Wang, Y. Yin, P. Stroeve, Y. Zhang, Z. Sheng, B. Cheng, K. Zhan, X. Hou, Dynamic curvature nanochannel-based membrane with anomalous ionic transport behaviors and reversible rectification switch, Adv. Mater. 31 (2019), 1805130.
[48] C. Chen, L. Hu, Nanoscale ion regulation in wood-based structures and their device applications, Adv. Mater. 33 (2020), 2002890.
[49] Q.Y. Wu, C. Wang, R. Wang, C. Chen, J. Gao, J. Dai, D. Liu, Z. Lin, L. Hu, Salinity-gradient power generation with ionized wood membranes, Adv. Energy Mater. 10 (2019), 1902590.

Yang Li received her Bachelor's degree from Shaanxi University of Science and Technology (SUST) in 2019, and now she is a current graduate student at South China University of Technology (SCUT). Her current research focuses on ionic woods and their new applications of moisture power generation and storage.

Jiedong Cui received his Bachelor's degree from Qilu University of Technology (Jinan, China) in 2019, and he is also a current graduate student at South China University of Technology (SCUT). His current research focuses on ionic conductive woods and their new applications of H_2O_2 production and electric-Fenton strategy.

Haoyu Shen received his Bachelor's degree from Northeast Forestry University (Harbin, China) in 2020, and he is currently a master student in South China University of Technology (SCUT). His current research mainly focuses on wood ionic conductors and its application in hygro-thermoelectric power generation.

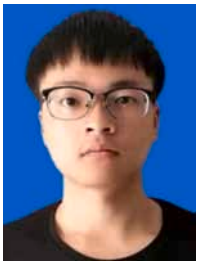

Chaocheng Liu received his Bachelor's degree from Inner Mongolia University of Technology (Hohhot, China) in 2020 and he is currently a master student South China University of Technology (SCUT). His current research focuses on the application of ionic wood materials for environmental purifications.

Peilin wu received her Bachelor's degree from Shaanxi University of Science and Technology (Shaanxi, China) in2021. She is currently a master student in the School of Light Industry Science and Engineering, South China University of Technology (SCUT), Guangdong Province. Her current research is mainly on the application of biomimetic nanostructures for ionic and electric conductors.

Zhiyun Qian received her Bachelor's degree from Xi'an University of Technology (ShaanXi, China) in 2021. And now she studies at South China University of Technology (SCUT) to achieve a master degree. Her current research mainly focuses on biomimetic solid ionic conductor for batteries and air purifications.

Yulong Duan received his Bachelor's degree from Qinghai University (Qinghai, China) in 2021. He is currently a master student in South China University of Technology (SCUT). His current research mainly focusses on biomimetic inorganic hygro-thermoelectric materials for power generation.

Detao Liu is currently an associate professor at the School of Light Industry and Engineering, South China University of Technology (SCUT). He received his Ph.D degree in sustainable wood and paper materials from South China University of Technology, Guangzhou, China in 2008. The main direction of his research is the sustainable environmental and energy materials by getting inspiration from natural biomass to create the biomimetic functional structures for advanced various applications in air & water protection and sustainable power for living and industrial environments.